Vol 18 No 5, May 2009
1674-1056/2009/18(05)/1833-05
Chinese Physics B
© 2009 Chin. Phys. Soc.
and IOP Publishing Ltd

Investigation of autoionization spectra of Sm atoms using an isolated-core excitation method*

Qin Wen-Jie(秦文杰), Dai Chang-Jian(戴长建)†,
Xiao Ying(肖 颖), and Zhao Hong-Ying(赵洪英)

Key Laboratory of Display Materials and Photoelectric Devices, Ministry of Education, Tianjin 300384, *China*

School of Science, Tianjin University of Technology, Tianjin 300384, *China*

(Received 31 August 2008; revised manuscript received 14 October 2008)

Using the isolated-core-excitation scheme and three-step laser resonance ionization spectroscopy approach, this paper, for the first time, has systematically investigated the autoionization spectra of atomic Sm, belonging to the $4f^6 6p nl$ and $4f^5 5d6s nl$ ($l = 0, 2$) configurations. In the experiment, the first two tunable dye lasers are employed to excite the Sm atom from its initial state to the different $4f^6 6s nl$ bound Rydberg states, then the third dye laser is scanned to drive the atom to the doubly-excited autoionizing states. With the above excitation scheme, the measured transition profiles of the autoionizing states are nearly symmetric, from which the level energies and widths can be easily obtained.

Keywords: isolated-core-excitation, autoionization spectra, Sm atom
PACC: 3280, 3280D, 3270J

1. Introduction

Investigation of atomic autoionizing states has recently received a lot of attention because it is related to many interesting phenomena, such as propagation without absorption[1] and coherent control.[2] In spite of numerous applications, information about the autoionizing states of the rare-earth atoms[3−9] is still scanty. Especially, only a few studies on the Sm atom have been reported.[10−13] The main reason for this can be explained by the very complex nature due to the fact that the 4f shell is only partially filled. Among the rare-earth atoms, the Yb atom has been most studied due to the fact that the 4f shell is completely filled. With only two s-electrons outside the closed shell, the spectrum of the Yb atom is basically an alkaline-earth-like spectrum. However, in the case of the Sm atom, with an unstable shell consisting of six 4f electrons, the spectrum contains the transitions of the electrons from both the outer $6s^2$ shell and the inner $4f^6$ shell. In addition, the seven fine structures of the same spectral term, $4f^6 6s^2\ {}^7F_J$, $J = 0-6$, are the lowest states of the Sm atom, which can be thermally populated by the temperature producing the Sm atomic beam in accordance with the Boltzman distribution; these states are the following: 21% ($^7F_0$), 37.8% ($^7F_1$), 25.5% ($^7F_2$), 10.9% ($^7F_3$), 3.6% ($^7F_4$), 1% ($^7F_5$), and 0.2% ($^7F_6$). It is the thermal population that makes the spectrum of the Sm atom even difficult, and prohibits one from obtaining the autoionization spectra by conventional spectral methods.

As one of the most powerful experimental methods, the isolated-core excitation (ICE) scheme[14] has been very successful in the study of the autoionizing states of the Ba atom.[15−17] Several major advantages of the ICE scheme are obvious: first, only low laser powers are required because all the transitions are single-electron transitions; second, it leads to a simplified autoionization spectrum whose profile is only determined by configuration interaction rather than by a combination of configuration interaction and interference effects, from which the information about the peak and width of a resonance can be easily obtained. Unlike the case for a Fano profile, the peak position and width of an observed spectrum with the ICE scheme can be interpreted as level energy and autoionization rate. In this work, we have made the first attempt to investigate the autoionizing states of atomic

*Project supported by the National Natural Science Foundation of China (Grant Nos 10574098 and 10674102) and the Natural Science Foundation of Tianjin of China (Grant No 05YFJMJC05200).
†Corresponding author. E-mail: daicj@126.com

Sm, converging to the $4f^6 6p$ and $4f^5 5d6s$ thresholds, using the ICE scheme.

In the following text, an introduction to the experimental approach is given in Section 2, the experimental results and discussion are presented in Section 3, and Section 4 gives the main conclusions.

2. Experimental

The experimental setup used here comprises three parts: a laser system, a vacuum chamber and a data acquisition system. All the lasers used here are manufactured by Quanta System: a Giant-770 model Nd:YAG pulsed laser and three D-100 model dye lasers. The vacuum chamber comprises an atomic oven and a micro-channel plate (MCP) detector. The data acquisition system, including a 4121B Model Boxcar and a 9650A Model digital pulse generator, is from the AMETEC company. A schematic diagram of the experimental setup is illustrated in Fig.1. The three dye lasers are pumped by harmonics of the same Nd:YAG pulsed laser. Except for the wavelength control, all three dye lasers are linearly polarized, and fixed to have the same parameters: pulse duration of 5–8 ns, energy of 100 μJ per pulse and line width of 0.1 cm^{-1}. The laser pulses of the second and third lasers are delayed from that of first laser by 10 ns and 20 ns, respectively, so that three laser pulses are sequential in time. The photons interact with Sm atoms in a vacuum chamber, where the atomic beam is made by a heating system. The atomic beam is collimated and directed to a region between two electric field plates, 1 cm apart, where it is crossed perpendicularly to the laser beams to reduce the Doppler broadening. About 0.5 μs after the laser pulses, a 100 V pulsed electric field is applied to the plates driving any ions resulting from the excitation and subsequent decay of the autoionizing states to a MCP detector, whose output is fed into a gated integrator. The analogue signal from the integrator is digitized with a Boxcar and stored in a computer for further analysis.

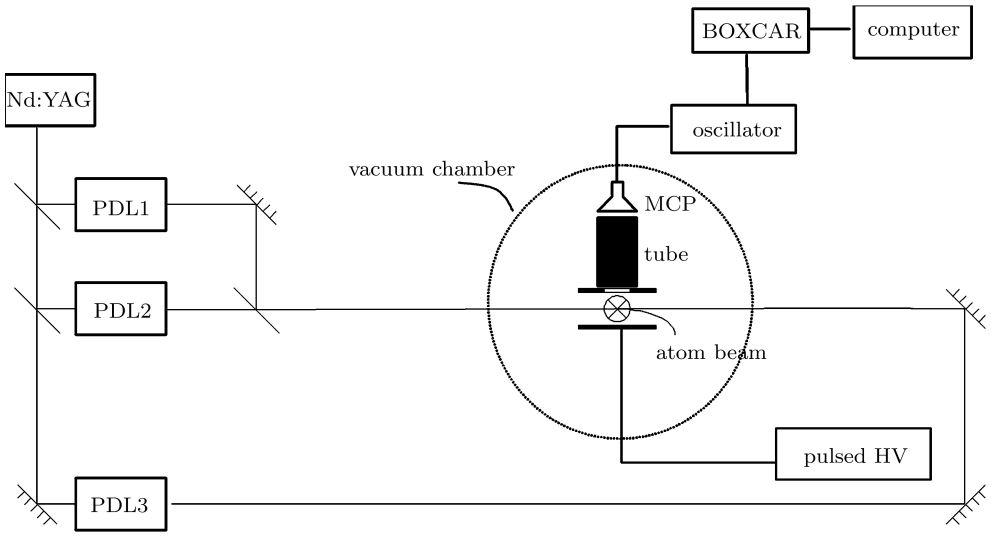


Fig.1. The schematic diagram of the experimental setup. It includes the pulsed dye lasers (PDLs), the atomic beam, and the detection systems. The atomic beam interacts with three laser beams in the vacuum chamber. The ion signal is detected by a MCP, averaged by a Boxcar, and sent into a computer for further analysis.

As mentioned before, at the working temperature of the Sm atomic beam, a significant population exists in the $^7F_1$ initial state whose energy is 292.58 cm^{-1},[18] which is compared with the other ground terms. Therefore, it is reliable to select transitions originating from the ground term with $J = 1$. The relevant energy levels and ICE scheme for the Sm atom autoionizing states are illustrated in Fig.2. In the first two steps the photons at wavelengths of λ_1 and λ_2 excite Sm atom from the initial state to the $4f^6 6s6p$ state, and then to the $4f^6 6snl$ ($l = 0, 2$) Rydberg states. The two-step excitation forms a state in which the outer nl electron is in an orbit

with a large radius far from the Sm^+ $4f^6 6s$ core. Then the third laser is scanned in the vicinity of the $4f^6 6s \rightarrow 4f^6 6p$ or $4f^6 6s \rightarrow 4f^5 5d6s$ transition of the Sm^+ ion core to drive the atom to the final $4f^6 6pnl$ or $4f^5 5d6snl$ autoionizing states, avoiding the excitation interference from the nl electron. Due to considerable interaction with underlying continua converging to the $4f^6 6s^+$or $4f^6 5d^+$ ionization limit, the atoms in the $4f^6 6pnl$ and $4f^5 5d6snl$ autoionizing states are very unstable, and thus quickly decay into an ion and an electron to the ionic states.

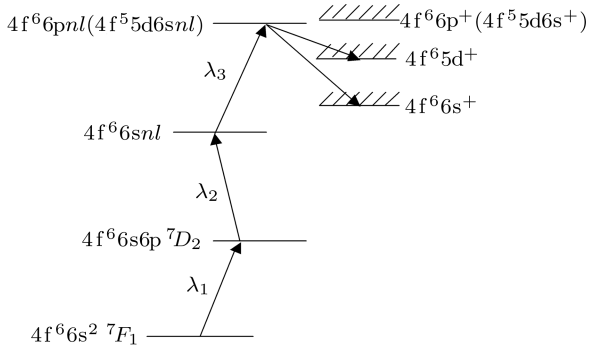


Fig.2. Isolated-core-excitation scheme used in the experiment. The first two tunable lasers at wavelengths of λ_1 and λ_2 excite the Sm atom from the initial state $4f^6 6s^2\ ^7F_1$ to the $4f^6 6snl$ ($l = 0, 2$) Rydberg states, then the third laser excites the core to the $4f^6 6p$ or $4f^5 5d6s$ state, producing the $4f^6 6pnl$ or $4f^5 5d6snl$ autoionizing state, which quickly decays into the $4f^6 6s^+$, $4f^6 5d^+$ ion states.

Since the core transition $4f^6 6s \rightarrow 4f^6 6p$ or $4f^6 6s \rightarrow 4f^5 5d6s$ is much stronger than that of the outer nl electron, the excitation of the nl electron can be neglected, thus the Beutler–Fano interference between the two excitation paths may be avoided. Therefore, the ICE scheme ensures an autoionization spectrum with a simplified Lorentzian profile.

3. Results and discussion

In this work, armed with the above equipment and technique, the spectra of the Sm atom $4f^6 6pnl$ and $4f^5 5d6snl$ autoionizing states are measured by scanning the wavelength of the third laser across the ion line transition from the $4f^6 6s \rightarrow 4f^6 6p$ and $4f^6 6s \rightarrow 4f^5 5d6s$ states while the first two lasers are set to pump different $4f^6 6snl$ bound Rydberg states. Most observed profiles are approximately Lorentzian and exhibit only one dominant feature. From the spectra we can conclude that the transition of Sm^+ $4f^6 6s \rightarrow 4f^6 6p$ and $4f^6 6s \rightarrow 4f^5 5d6s$ overwhelmingly dominate the direct photoionization process (e.g. $4f^6 6snl \rightarrow 4f^6 6s\varepsilon l'$ transition), eliminating the possible interference between the two pathways of excitation. Therefore, during the process of third-step excitation, the nl electron basically acts like a spectator, which is one of the advantages of the ICE scheme. To confirm this speculation, we have fitted the observed spectra to the Lorentzian profiles, two examples of many experimental spectra are presented in Figs.3 and 4, for the spectra of the $4f^6 6pnl$ and $4f^5 5d6snl$ autoionizing states, respectively. However, for the unusual spectra with multi-peak profiles, we have to fit them to multi-Lorentzian profiles, for example, the spectra of autoionizing states shown in Fig.5, whose profiles can be obtained by fitting the spectra to multi-Lorentzian profiles. The abscissa represents the photon energy of the third laser and the dashed curves in the figures are the best fits to the Lorentzian profiles.

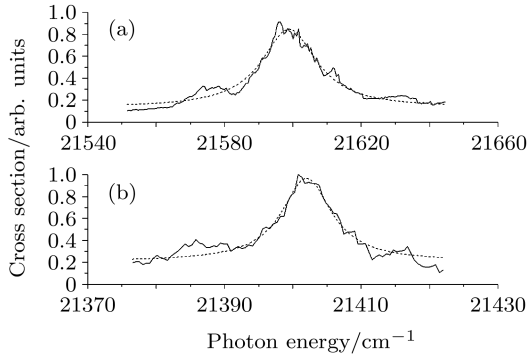


Fig.3. Lorentzian-profile-fitting results for experimental spectra. The solid lines represent the experimental spectra, while the dashed lines are from the Lorentzian fitting. (a) The third laser crosses the $4f^6(^7F)6s\ J = 5/2 \rightarrow 4f^6(^7F)6p\ J = 5/2$ resonance transition; (b) the third laser crosses the $4f^6(^7F)6s\ J = 7/2 \rightarrow 4f^6(^7F)6p\ J = 7/2$ resonance transition.

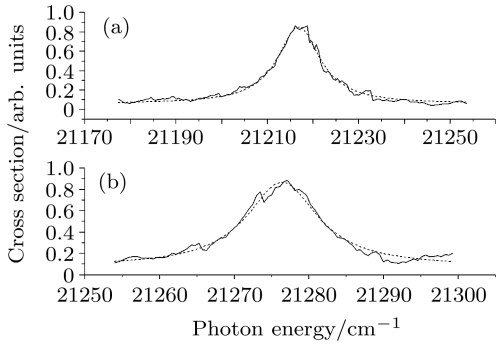


Fig.4. The same as Fig.3, but (a) the third laser crosses the $4f^6(^7F)6s\ J = 5/2 \rightarrow 4f^5(^6H^o)5d6s\ J = 5/2$ resonance transition; (b) the third laser crosses the $4f^6(^7F)6s\ J = 7/2 \rightarrow 4f^5(^6H^o)5d6s\ J = 7/2$ resonance transition.

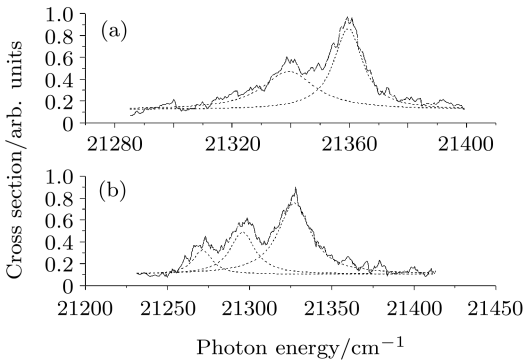


Fig.5. Multi-Lorentzian-profile fitting results for several experimental spectra. The solid lines represent the experimental spectrum, while the dashed lines are from the Lorentzian fitting. (a) The single-Lorentzian profiles in the blue side represent the third laser crossing the $4f^6(^7F)6s\ J = 7/2 \rightarrow 4f^6(^7F)6p\ J = 7/2$ resonance transition; those in the red side represent the third laser crossing the $4f^6(^7F)6s\ J = 3/2 \rightarrow 4f^6(^7F)6p\ J = 3/2$ resonance transition. (b) The single-Lorentzian profiles in the blue side represent the third laser crossing the $4f^6(^7F)6s\ J = 3/2 \rightarrow 4f^6(^7F)6p\ J = 1/2$ resonance transition; those in the middle represent the third laser crossing the $4f^6(^7F)6s\ J = 7/2 \rightarrow 4f^5(^6H^o)5d6s\ J = 7/2$ resonance transition; those in the red side represent the third laser crossing the $4f^6(^7F)6s\ J = 1/2 \rightarrow 4f^6(^7F)6p\ J = 1/2$ resonance transition.

It is worthwhile to point out that our investigations cover an energy range that has not been explored before. As mentioned before, the primary objectives of this work are determining the level energies and widths of the autoionizing states. Taking advantage of the ICE method, we can obtain the experimental level energies and widths of autoionization spectra by fitting the data to Lorentzian profiles, instead of obtaining them directly from the experimental ones. This treatment enables us to obtain the desired data more accurately from the experimental spectra. The level energies E and widths Γ for the $4f^6 6p nl$ and $4f^5 5d6s nl$ autoionizing states are measured and tabulated in Tables 1–2 and 3–4, respectively.

In order to make the above-mentioned level energies and widths physically meaningful, let us examine the process of obtaining them. Since three photons are necessary to reach an autoionizing state, one must add the energy of peak position, obtained from an autoionization spectrum, to the energy of the bound $4f^6 6s nl$ state, excited by the first two photons. Note that the data in Table 2 with serial no.9 are obtained by double-Lorentzian-profile fittings, from which the data of $4f^6 6p nl$ with the third laser crossing the $4f^6\,(^7F)6s J = 3/2 \rightarrow 4f^6\,(^7F)\,6p' J = 3/2$ resonance transition are obtained simultaneously, the

Table 1. Level energies (E) and widths (Γ) of $4f^6 6p nl$ autoionizing states converging to the $4f^6(^7F)6p\ J = 5/2$ limit at 67948.49 cm^{-1}, λ_3 across the $4f^6(^7F)6s\ J = 5/2 \rightarrow 4f^6(^7F)6p\ J = 5/2$ resonance transition.

serial No.	E/cm^{-1}	Γ/cm^{-1}
1	62098.44±0.15	39.64±0.10
2	62405.82±0.25	32.22±0.25
3	62475.10±0.10	20.06±0.10
4	62543.53±0.20	21.64±0.15
5	62826.82±0.15	20.20±0.15
6	64080.22±0.30	28.37±0.20
7	64885.69±0.25	17.73±0.20
8	65047.19±0.30	33.27±0.30
9	65499.53±0.10	13.87±0.10
10	66180.52±0.10	18.00±0.10

Table 2. Level energies (E) and widths (Γ) of $4f^6 6p nl$ autoionizing states converging to the $4f^6(^7F)6p\ J = 7/2$ limit at 68394.41 cm^{-1}, λ_3 across the $4f^6(^7F)6s\ J = 7/2 \rightarrow 4f^6(^7F)6p\ J = 7/2$ resonance transition.

serial No.	E/cm^{-1}	Γ/cm^{-1}
1	61779.62±0.20	25.67±0.10
2	62072.46±0.20	111.13±0.20
3	62734.47±0.20	46.99±0.20
4	63218.24±0.25	71.89±0.20
5	64155.09±0.15	18.69±0.15
6	64283.83±0.20	16.30±0.15
7	65513.68±0.10	13.02±0.10
8	66048.20±0.10	8.53±0.10
9	66118.46±0.15	21.45±0.15
10	66139.00±0.15	11.70±0.10

Table 3. Level energies (E) and widths (Γ) of $4f^5 5d6s nl$ autoionizing states converging to the $4f^5(^6H^o)5d6s\ J = 5/2$ limit at 67558.98 cm^{-1}, λ_3 across the $4f^6(^7F)6s\ J = 5/2 \rightarrow 4f^5(^6H^o)5d6s\ J = 5/2$ resonance transition.

serial No.	E/cm^{-1}	Γ/cm^{-1}
1	61694.14±0.25	27.53±0.25
2	61870.09±0.25	13.16±0.25
3	61883.01±0.20	34.43±0.20
4	62056.17±0.10	14.93±0.10
5	62891.30±0.30	20.76±0.20
6	63037.99±0.30	96.16±0.30
7	63087.02±0.30	55.17±0.30
8	63742.84±0.20	66.08±0.20
9	64082.99±0.25	15.15±0.25
10	64622.92±0.30	32.68±0.30
11	64639.19±0.20	82.09±0.20
12	65443.15±0.20	15.67±0.20
13	65800.26±0.10	11.12±0.10

Table 4. Level energies (E) and widths (Γ) of $4f^5 5d6snl$ autoionizing states converging to the $4f^5(^6H^o)5d6s$ J=7/2 limit at 68307.68 cm^{-1}, λ_3 across the $4f^6(^7F)6s$ $J = 7/2 \rightarrow 4f^5(^6H^o)5d6s$ $J = 7/2$ resonance transition.

serial No.	E/cm^{-1}	Γ/cm^{-1}
1	62134.17±0.20	34.39±0.20
2	63142.96±0.15	37.38±0.15
3	63709.01±0.10	24.35±0.10
4	64347.16±0.30	19.88±0.30
5	64594.22±0.30	116.53±0.30
6	64724.62±0.30	25.74±0.30
7	65221.12±0.25	14.15±0.25
8	65229.28±0.10	7.86±0.10
9	65280.19±0.15	17.47±0.15
10	65306.01±0.10	17.90±0.10

energy and width are 66138.76 and 11.82 cm^{-1}, respectively. The data in Table 4 with serial no.10 are obtained by multi-Lorentzian-profile fittings, from which the data of $4f^6 6pnl$ with the third laser crossing the $4f^6(^7F)6s$ $J = 1/2 \rightarrow 4f^6(^7F)6p$ $J = 1/2$ resonance transition and the data of $4f^6 6pnl$ with the third laser crossing the $4f^6(^7F)6s$ $J = 3/2 \rightarrow 4f^6(^7F)6p$ $J = 1/2$ resonance transition are obtained simultaneously. Namely, their energies and widths are 65283.32 and 13.51 cm^{-1} and 65337.91 and 23.48 cm^{-1}, respectively. On the other hand, the width of an autoionizing state represents the total autoionization rate to all possible continuum states, so, the width indicates the coupling strength of an autoionizing state with the underlying continua.

Finally, it is important to note that the same scheme can be utilized to detect bound Rydberg states once we have mastered the information about the autoionization spectrum, using the same setup shown in Fig.1. Instead of scanning the wavelength of the third laser, the wavelength of the second laser is tuned while fixing the wavelength of third laser near the Sm^+ $4f^6 6s \rightarrow 4f^6 6p$ or $4f^6 6s \rightarrow 4f^5 5d6s$ resonance transition. This method has proven to be very versatile in detecting both the low and high-lying members of a Rydberg series.

4. Conclusion

In this paper, we have presented the results of our recent investigation of the atomic Sm $4f^6 6pnl$ and $4f^5 5d6snl$ autoionizing states for the first time. The transition profiles excited by the ICE scheme show a high degree of symmetry, from which the peak positions and widths of the resonance can be easily obtained, resulting in the information about level energies and autoionization rates of given autoionizing states. On the basis of this advanced excitation technique, it is not surprising that more reliable and accurate evidence about the physical characteristics of complex atoms can be obtained. Since all the data are obtained for the first time, they will greatly enrich our knowledge on the atomic spectroscopy of the Sm atom.

References

[1] Paspalakis E, Kylstra N J and Knight P L 1999 *Phys. Rev.* A **60** 642

[2] Lyras A and Bauchau H 1999 *Phys. Rev.* A **60** 4781

[3] Bhattacharyya S, Nakhate S G, Jayasekharan and Razvi M A N 2006 *Phys. Rev.* A **73** 062506

[4] Bhattacharyya S, Razvi M A N, Cohen S and Nakhate S G 2007 *Phys. Rev.* A **76** 012502

[5] Ogawa Y and Kujirai O 1999 *J. Phys. Soc. Jpn.* **68** 428

[6] Bhattacharyya S, Souza R D, Rao P M and Razvi M A N 2003 *Spectrochim Acta* Part B **58** 469

[7] Yi J H and Lee J 1995 *Phys. Rev.* A **51** 3053

[8] Zhou H J, Xu X Y, Huang W, Li L Q and Chen D Y 1992 *Chin. Phys.* **1** 19

[9] Zhou H J, Xu X Y, Huang W and Chen D Y 1993 *Chin. Phys.* **2** 917

[10] Hu S F, Mei S M, Zhang S, Chen X and Xu Y F 1989 *Chin. Phys. Lett.* **6** 64

[11] Park H, Kim H C, Yi J, Han J, Rhee Y J and Lee J 1998 *J. Korean. Phys. Soc.* **33** 288

[12] Jayasekharan T, Razvi M A N and Bhale G L 2000 *J. Phys.* B: *At. Mol. Opt. Phys.* **33** 3123

[13] Kujirai O and Ogawa Y 2003 *J. Phys. Soc. Jpn.* **72** 1057

[14] Cooke W E, Gallagher T F, Edelstein S A and Hill R M 1977 *Phys. Rev. Lett.* **40** 178

[15] Li S B, Dai C J, Sun W and Xue P 2001 *J. Phys.* B: *At. Mol. Opt. Phys.* **34** 2123

[16] Zhang Y, Dai C J and Li S B 2004 *J. Electron Spectrosc. Relat. Phenom* **135** 63

[17] Li S B and Dai C J 2003 *J. Quant. Spectrosc. Radiat. Transfer* **77** 345

[18] Martin W C, Zalubas R and Hagan L 1978 *Atomic Energy Levels-The Rare-Earth Elements* (Washington: National Bureau of Standards) p162